PAPER

Check for updates

Ascorbic acid-induced fiber-scrolling of titanium carbide Ti₃C₂Tₓ MXene†

Jinxin Cao,[a] Yuru Wang,[a] Bingqing Wei, [ID] [b] Jiaxin Ye[c] and Qing Zhang [ID] *[a]

Changing the morphology of two-dimensional materials often offers an efficient and effective means to exploit their electronic and mechanical properties. Two-dimensional materials such as graphene can be scrolled into one-dimensional fibers *via* simple sonication. Unfortunately, scrolling MXene nanosheets into fibers is quite challenging, especially $Ti_3C_2T_x$ composed of three layers of titanium atoms and two layers of carbon atoms. Herein, we report a new method to fabricate MXene fibers *via* ascorbic acid (AA) induced scrolling of $Ti_3C_2T_x$ nanosheets. An unusual AA-$Ti_3C_2T_x$ interaction is discovered in that intercalated AA molecules bind to and interact with the $Ti_3C_2T_x$ surface in the form of a hydrogen bonding-bonded assembly instead of as individual molecules, and a sheet-scrolling mechanism is proposed based on this interaction. The as-obtained MXene fibers exhibit a compact cross-section, and the diameter can be tailored from hundreds of nanometers to several micrometers through tuning the MXene/AA ratio. Moreover, the storage modulus of the MXene-fiber sponge attains its maximum value of ~1 MPa when a unique morphology comprising both fibers and not-yet-scrolled sheets is presented. This work offers a new strategy of fiber-shaping MXenes for applications in structural composites and flexible electronics.

1. Introduction

Materials with high Young's modulus, such as defect-free graphene with Young's modulus of about 1 TPa and reduced graphene oxide with Young's modulus of 0.25 ± 0.15 TPa,[1] are potential candidates for applications in structural composites, protective coatings, fibers, *etc.*[2] Transition metal carbides, carbonitrides, and nitrides (MXenes), with a chemical formula of $M_{n+1}X_nT_x$ and over 20 species discovered so far,[3,4] are a large family of two-dimensional materials besides graphene,[5,6] boron nitride,[7] and transition metal dichalcogenides,[8] where M stands for a transition metal (such as Ti, V, Nb, Mo, Cr, *etc.*), X is carbon or nitrogen, and T_x represents the surface terminations (–O, –OH, –F).[4,9] MXenes have attracted research in diverse fields, including energy storage (batteries and supercapacitors),[10–13] structural composites,[14] electro-catalysis,[15–17] and electromagnetic interference shielding[18,19] owing to their high metallic conductivity,[20] abundant functional surface terminations,[11] and excellent hydrophilicity.[15] Unlike graphene, which is constructed of one-layer sp²-bonded carbon atoms,[6] MXenes

contain multiple layers of metal atoms and carbon/nitrogen atoms. Taking the first reported MXene $Ti_3C_2T_x$ as an example, a single layer $Ti_3C_2T_x$ includes 3 layers of titanium atoms together with 2 layers of carbon atoms, and Young's modulus of a single layer of $Ti_3C_2T_x$ is reported to be 0.33 ± 0.03 TPa,[1] which is the highest among solution-processed two-dimensional materials, demonstrating exceptional mechanical stiffness and rigidity.

Due to the exceptional mechanical and electrical properties exhibited by MXenes, extensive attempts have been made to transform the morphology of two-dimensional MXene nanosheets into one-dimensional MXene fibers for applications in wearable or flexible electronics. So far, MXene has been used as a coating agent on other fibers such as carbon fibers or optical fibers,[14,21] or fabricated into fibers through electrospinning or wet spinning methods after mixing with carbon nanotubes or graphene as well as polymeric binders such as poly(3,4-ethylenedioxythiophene): polystyrene sulfonate (PEDOT:PSS), polyacrylonitrile (PAN) or polycaprolactone (PCL).[22–26] Additive-free MXene fibers have recently been produced utilizing the nematic liquid crystalline phases of MXenes, which show an excellent electrical conductivity of up to ~7750 S cm⁻¹.[27,28] However, for all the fiber-shaped MXenes above, the MXene sheets contained-in are stacked together instead of scrolling up, with their two-dimensional flat-sheet feature preserved.

Two-dimensional materials with large lateral sizes usually tend to crease or even scroll up into nanoscrolls under certain conditions, such as nanoscrolled graphene produced by simple

[a]Institutes of Physical Science and Information Technology, Anhui University, Hefei, 230039, Anhui, China. E-mail: zhangq@ahu.edu.cn

[b]Department of Mechanical Engineering, University of Delaware, Newark, Delaware, 19716, USA

[c]School of Mechanical Engineering, Hefei University of Technology, Hefei, 230009, Anhui, China

† Electronic supplementary information (ESI) available. See https://doi.org/10.1039/d2ra03174d

sonication and freeze-drying.[29,30] Nonetheless, sonication leads to exfoliation or the decrease in the lateral size of MXene sheets instead of scrolling.[31,32] Nanoscrolls of MXenes, especially that of $Ti_3C_2T_x$, have rarely been reported. Fang *et al.* reported on a hollow-tube-like Ti_2CT_x (with an outer diameter of ~1 μm) *via* spray-lyophilization while under the same condition, only bubble-like $Ti_3C_2T_x$ were obtained, demonstrating the difficulty in scrolling up MXene sheets.[33] Vaughn *et al.* also reported on Ti_2CT_x scrolls under sonication in the presence of *p*-phosphonic acid calix[n]arenes.[34] So far, only Naguib *et al.* observed evidence of nanoscrolls of $Ti_3C_2T_x$ MXene with TEM (transmission electron microscopy),[9] and Meng *et al.* reported on folding $Ti_3C_2T_x$ sheets into loosely packed strips after a 7 day-long freeze-drying process with the addition of NH_4OH.[35]

Herein, we demonstrate for the first time that two-dimensional $Ti_3C_2T_x$ MXene nanosheets can be scrolled up into one-dimensional fibers in ascorbic acid (AA) under sonication, where AA is one of the common antioxidants used for MXene preservation.[36–38] The successful scrolling and fiber-formation rely upon two bonds: the coordination bond that binds AA to $Ti_3C_2T_x$ surface and the hydrogen bond between AA molecules. This particular AA-induced scrolling of $Ti_3C_2T_x$ MXene will provide a novel strategy to fabricate MXene fibers to explore their potential applications in wearable or stretchable electronic devices.

2. Results and discussion

2.1 Fabrication of $Ti_3C_2T_x$ scrolled fibers

$Ti_3C_2T_x$ nanosheets of one or two layers thick (Fig. S1†) are mixed with AA to different ratios. After simple sonication treatment in the iced bath and around one-day freeze-drying, sponge-like AA-treated $Ti_3C_2T_x$ MXene samples are obtained (Fig. S2,† denoted as $M_{10}AA_x$, 10 : x is the weight ratio of $Ti_3C_2T_x$ MXene to AA, and x is called the AA ratio in the following discussion). The as-obtained MXene sponges have substantially different microstructures from previously reported $Ti_3C_2T_x$ MXene prepared from the similar sonication and freeze-drying procedure which normally contain only two-dimensional sheets.[38]

Fig. 1a schematically depicts the transformation process of $Ti_3C_2T_x$ MXene from two-dimensional sheets into one-dimensional fibers based on the SEM observations (Fig. 1b), and the as-obtained fibers are filled instead of presenting hollow-tube-like features (Fig. 1c and d). As shown in Fig. 1b, the morphology transformation process from flat sheets to fibers can be roughly divided into four steps as the AA ratio increases: with no AA addition, the flat-sheet feature is preserved in pristine $Ti_3C_2T_x$ ($M_{10}AA_0$), and that neither scrolling nor twisting occurs. This is the initial step (step I). As AA ratio increases (from $M_{10}AA_1$ to $M_{10}AA_8$), the $Ti_3C_2T_x$ sheets start to roll up and twist into strips, denoted as step II (Fig. S3†). When the AA ratio reaches 10 : 10, tightly structured fibers first appear (with some sheets wrapped around as in Fig. 2a), this is step III. As the AA ratio continues to increase, several fibers bind and twine around each other to form an even thicker "bundle" of fibers. This is the last, step IV. During the transformation

process, there are three major types of actions: the first is the scrolling and twisting of MXene sheets into long strips, the second is the wrapping of MXene sheets around the strips and fibers and the last action is fibers twining together. Moreover, the diameter of the fibers is tunable, from less than 500 nm for $M_{10}AA_{10}$ fibers to larger than 3 μm for $M_{10}AA_{25}$ fibers (Fig. 2a–d). On the other hand, previously reported MXene fibers fabricated by the wet-spinning method usually admit a diameter of tens of micrometers.[24–26,28]

2.2 Characteristics of $Ti_3C_2T_x$ scrolled fibers

The X-ray diffraction characterization results (XRD, Fig. 2e and f) present a progressive intercalation process of AA molecules into the interlayer spacing of $Ti_3C_2T_x$ (especially the asterisked peaks in $M_{10}AA_2$ and $M_{10}AA_4$). The pristine MXene, *i.e.*, the $M_{10}AA_0$, admits a (002) peak at $2\theta \sim 7.02°$, corresponding to a basal spacing $d_{(002)}$ of 1.26 nm.[20] During increasing the AA ratio from 0 to 10, the (002) peak gradually shifts to the left, and the $d_{(002)}$ expands and reaches its maximum at ~1.93 nm ($2\theta \sim 4.59°$). Interestingly, a broad shoulder emerges on the left side of the (002) peak since $M_{10}AA_{10}$ and for the rest $M_{10}AA_x$ samples with higher AA ratios which contain fibers (Fig. 2f, shaded area), while it is missing for those with lower AA ratios and have only twisted strips. This broad shoulder might be ascribed to the compact structure of the as-obtained fibers (Fig. 1c and d) as $Ti_3C_2T_x$ sheets wrapping tightly over strips and fibers, and the resultant compact structure gives rise to the shoulder on the left side of the (002) peak. The appearance of this broad shoulder could be considered a characteristic and feature indicator of the successful formation of $Ti_3C_2T_x$ fibers. Moreover, this broad shoulder further demonstrates that the fibers are filled and compacted, not hollow or loose. The intercalation of AA molecules into the interlayer spacing is also demonstrated with the TEM result (Fig. 2g), where the intercalated AA molecules show as a thin "line" between two layers of $Ti_3C_2T_x$ and expands the d-spacing to ~2.0 nm, consistent with the XRD results (d-spacing of only ~1.07 nm is also observed in the upper-right part of Fig. 2g, where there is no AA intercalation).

$Ti_3C_2T_x$ MXenes can disperse and form stable colloidal solution in water instead of agglomerating and precipitating, mainly owing to the negatively charged nanosheets (zeta potential value locates around −40 mV).[39] Reducing the negative charge could lead to agglomeration and sedimentation. As shown in Fig. 3a, after AA addition, there is a diminishing of zeta potential; consequently, the electrostatic repulsion is attenuated between the neighboring nanosheets and within the single nanosheet. Therefore, it is reasonable to conjecture that the diminishing of zeta potential after AA addition could be one of the reasons for scrolling MXene nanosheets as reducing the intra-sheet electrostatic repulsion.

To further explore the effects of zeta potential, sodium bicarbonate $NaHCO_3$ titration on $M_{10}AA_{10}$ is carried out. $NaHCO_3$ is a weak base salt and can react with AA to produce sodium ascorbate, which also is used as an antioxidant for MXenes.[36,37] Here, we use pH to describe the amount of $NaHCO_3$ titrated. The starting pH of the $M_{10}AA_{10}$ solution is 3.4. After

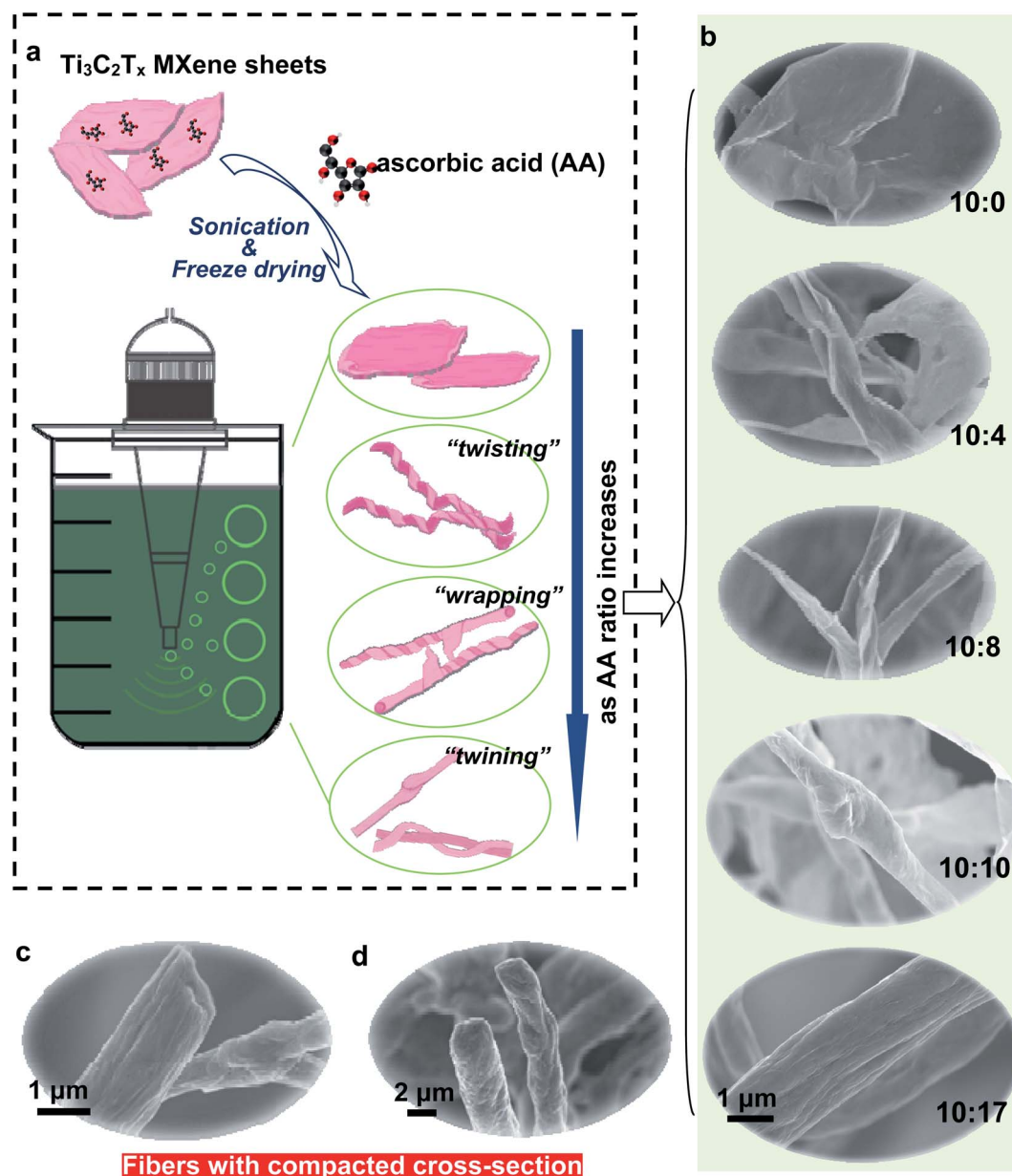**Fig. 1** (a) The schematic illustration of the AA treatment process and the scrolling-up process of $Ti_3C_2T_x$ Mxene nanosheets; (b) SEM images of AA-treated MXene ($M_{10}AA_x$) with increasing AA ratios presenting different stages from flat sheets to tightly scrolled fibers during the scrolling-up process; SEM images of (c) $M_{10}AA_{17}$ and (d) $M_{10}AA_{25}$ both presenting a compacted cross-section.

adding $NaHCO_3$ to pH = 4, almost all MXene fibers disappear (Fig. 3c); meanwhile, the zeta potential changes drastically from around −27 mV to around −39 mV, and the d-spacing $d_{(002)}$ decreases a little from 1.97 nm to 1.74 nm (Fig. 3a and b), corroborating the conjecture that zeta potential (and/or AA intercalation) is crucial for the fiber formation that even minor adjustment with $NaHCO_3$ could lead to failure. As continues adding $NaHCO_3$, a fiber-unfolding process is vividly presented: from a few fibers left at pH 4 (Fig. 3c, blue circled area), to a large curved surface at pH 5, to a flat surface at pH 7, then MXene agglomerates to thick chunks at pH 8 (Fig. S4†). The d-spacing keeps decreasing as adding $NaHCO_3$ to pH ∼ 5. This de-intercalation should be the result of the neutralization reaction

between $NaHCO_3$ and AA, yet merely partial de-intercalation can be achieved through adding $NaHCO_3$ as d-spacing stops decreasing at pH ∼ 5 and stays at ∼1.6 nm. Moreover, all unfolded MXene sheets exhibit corrugated surfaces (Fig. 3c and S4†), possibly resulting from the previous scrolling process.

Moreover, a control experiment of hydrochloric acid (HCl) treated MXene rules out the effects of the pH environment on the scrolling of MXene nanosheets. As shown in Fig. 3a and b, HCl only changes the pH yet does not affect the zeta potential or the d-spacing, and the MXene sheets do not scroll (Fig. 3d). Furthermore, acetic acid (HAc) treatment demonstrates that tuning zeta potential alone does not scroll up the MXene nanosheets either. As shown in Fig. 3a, HAc-treated MXene
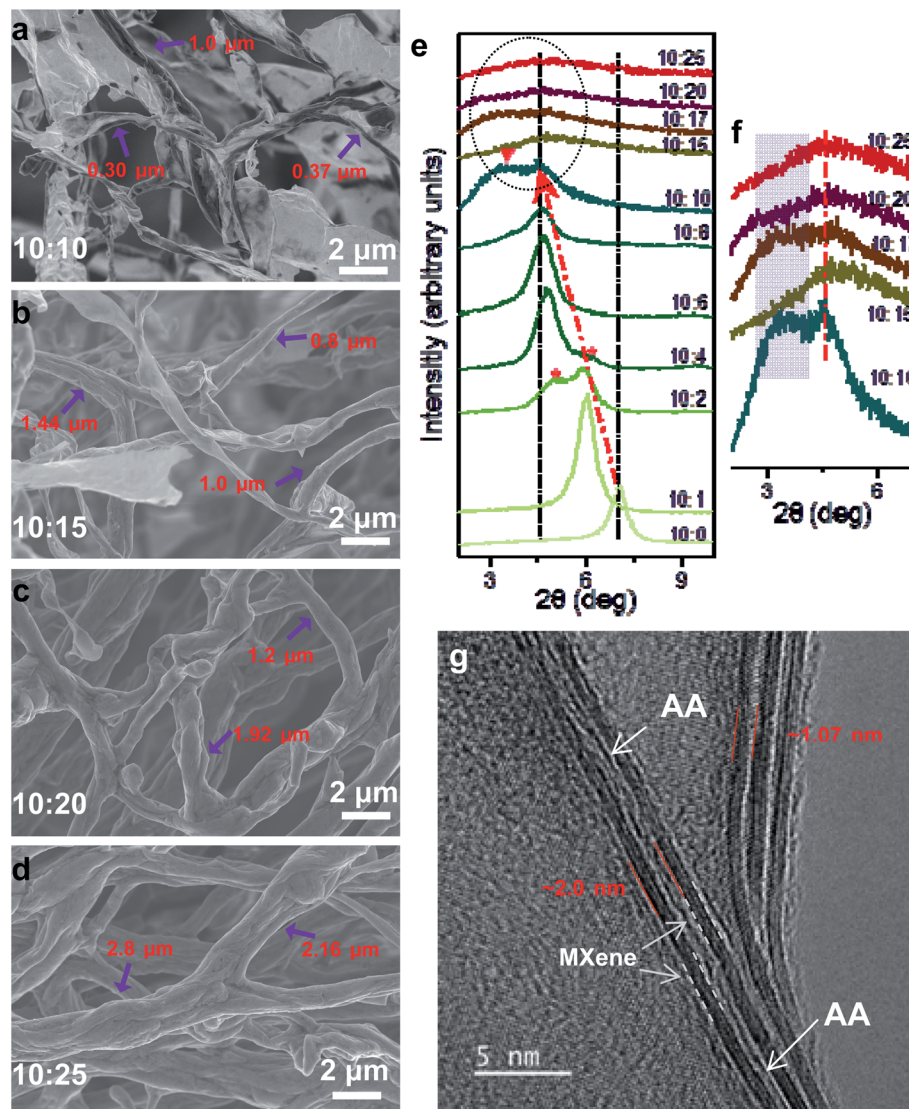
Paper

Fig. 2 SEM images of (a) $M_{10}AA_{10}$ (with the purple arrows pointing at the fibers), (b) $M_{10}AA_{15}$, (c) $M_{10}AA_{20}$ and (d) $M_{10}AA_{25}$, showing increasing fiber diameter; (e) and (f) XRD results of M_xAA_y showing (002) peak position variation with AA ratios; (g) TEM image of $M_{10}AA_{10}$.

admits a zeta potential around −32 mV, close to that of AA-treated MXene, while the XRD result (Fig. 3b) demonstrates that no intercalation happens. The HAc-treated MXene sheets have a corrugated surface (Fig. 3e). Tuning zeta potential could corrugate the sheets but is not enough to scroll up them into nanoscrolls.

How come intercalation contributes to scrolling and fiber formation of $Ti_3C_2T_x$ MXene? X-ray photoelectron spectroscopy (XPS) analysis on the AA-treated MXenes reveals that not only AA molecules can be intercalated and expand the interlayer spacing of $Ti_3C_2T_x$ like many other compounds such as DMF, DMSO, etc.,[40] but also interact with the atomic structure of $Ti_3C_2T_x$ and bind to the surface titanium atoms.

As shown in Fig. 4a, the C 1s spectrum of $M_{10}AA_0$ without AA treatment shows four peaks: C–Ti (∼282.22 eV), C–Ti-T_x (∼283.01 eV), graphitic C–C (∼284.81 eV), and C–O (∼286.29 eV). The former two are the characteristic peaks of $Ti_3C_2T_x$,

while the graphitic C–C and C–O should result from the solvents or the exposure of the material to the ambient environment during the preparation process.[41,42] As for $M_{10}AA_{10}$, three additional peaks appear at ∼286.95 eV, ∼288.68 eV, and ∼291.93 eV. The peak at ∼288.68 eV is assigned to O–C=O, together with the increase of the C–O peak fraction from 12.42% to 28.75% (Table S1†), both should come from the carbon structure of AA molecules. The peak at ∼291.93 eV is assigned to C–F, possibly formed between the carbon atom on AA or graphitic carbons, and the surface termination –F of $Ti_3C_2T_x$.[43] According to previous studies, the catechol groups and their derivatives tend to bind strongly to titanium atoms through a catechol-titanium coordination bond C–O–Ti.[41,44] The appearance of the peak at ∼286.95 eV is assigned to a catechol-titanium coordination bond between AA and $Ti_3C_2T_x$. In addition, downshifts toward lower binding energies are monitored for C–Ti (∼281.99 eV), and C–Ti–T_x (∼282.95 eV), suggesting the electron transfer from
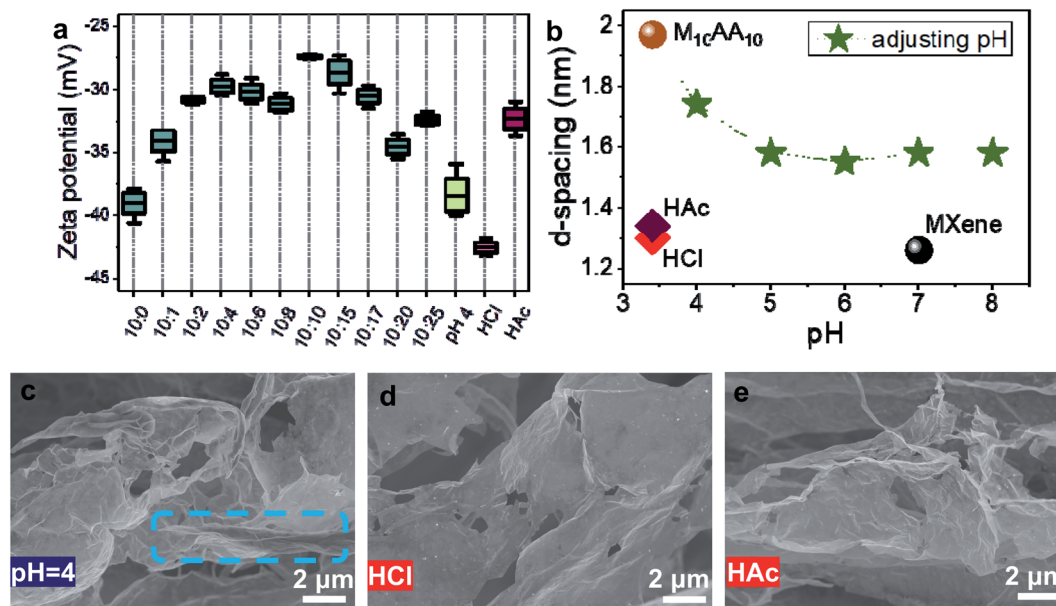
Fig. 3 (a) Zeta potential of $M_{10}AA_x$ with different AA ratios as well as $M_{10}AA_{10}$ with pH adjusted to 4 using $NaHCO_3$, MXene treated with HCl, and HAc; (b) XRD results of $M_{10}AA_{10}$ treated with $NaHCO_3$ to different pH values, MXene treated with HCl, and HAc; (c) SEM image of $M_{10}AA_{10}$ with pH adjusted to 4 (the blue circled area is a remaining fiber); SEM images of MXene treated with HCl (d) and with HAc (e).
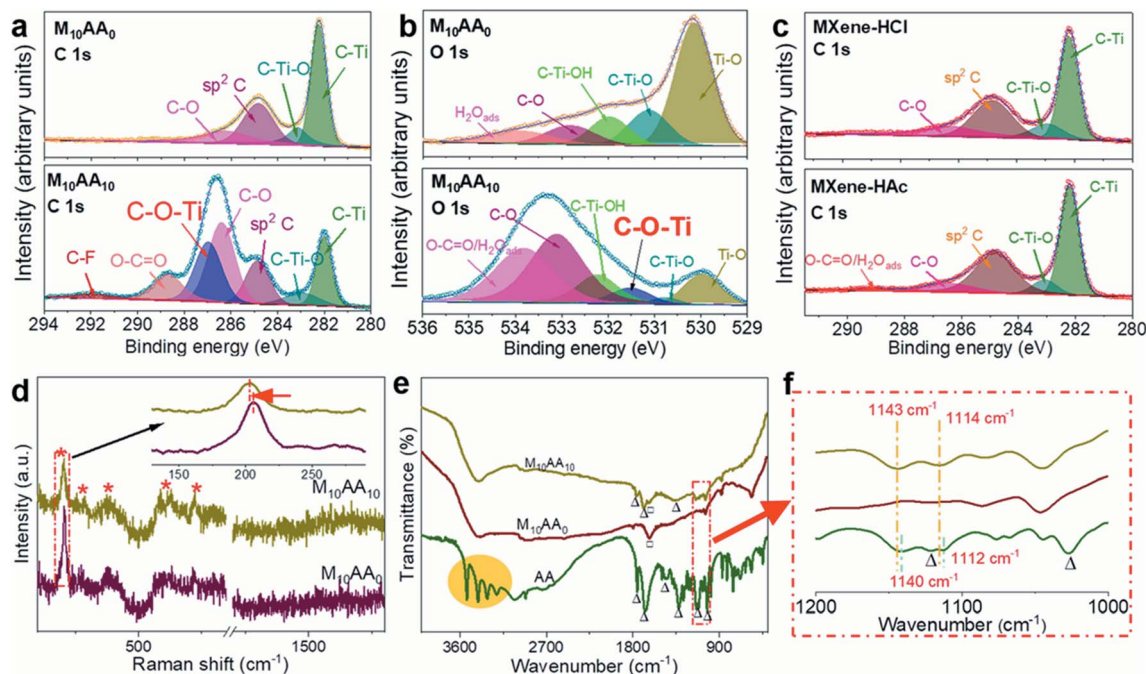

Fig. 4 (a) High-resolution C 1s spectra and (b) O 1s spectra of $M_{10}AA_0$ and $M_{10}AA_{10}$; (c) high-resolution C 1s spectra of MXene treated with HCl and with HAc; (d) Raman spectra of $M_{10}AA_0$ and $M_{10}AA_{10}$; (e) and (f) FTIR spectra of $M_{10}AA_0$, $M_{10}AA_{10}$ and AA (where "Δ" stands for characteristic peaks for AA and "$\square$" for $Ti_3C_2T_x$ MXene, details on the assignment of FTIR peaks are given in Fig. S6c†).

AA to MXene due to the C–O–Ti charge–transfer complex.[41] The O 1s spectrum also proves the existence of C–O–Ti with a deconvoluted peak at ~531.5 eV, also assigned to C–O–Ti (Fig. 4b).[41,45] The slight downshift of deconvoluted O 1s peaks for MXene (Ti–O and C–Ti–O) is consistent with C 1s (Table

S1†). The C–O–Ti peak is not presented in HCl or HAc treated MXenes (Fig. 4c and S5†).

Raman spectra indicate a slight red shift (~2.06 cm^{-1}, Fig. S6b†) upon AA intercalation for the peak at ~206 cm^{-1} (Fig. 4d). This peak corresponds to A_{1g}, an out-of-plane vibration of Ti and C atoms.[46] This redshift, together with the appearance of

© 2022 The Author(s). Published by the Royal Society of Chemistry

FTIR peaks at 1114 cm^{-1} and 1143 cm^{-1} in $M_{10}AA_{10}$, which are located close to the C–O–C stretching vibration of AA around 1112 cm^{-1} and 1140 cm^{-1}, yet slightly shifted to higher wavenumbers (Fig. 4e and f), can both be addressed as the results of the formation of catechol-titanium bonding and charge–transfer complex at the MXene surfaces.[41,47] Most interestingly, for pure AA, sharp peaks near 3500 cm^{-1} are observed from its FTIR spectrum and attributed to the –OH group without hydrogen bonding; while in $M_{10}AA_{10}$, those sharp peaks are substituted by a broad peak, which possibly originates from the polarity changes of –OH group as induced by hydrogen bonding between the –OH and –C=O groups in AA,[48,49] suggesting AA molecules could self-assemble together, forming an orderly assembly *via* significant intermolecular hydrogen bonding. This is consistent with the TEM results (Fig. 2g), representing AA lines as multiple AA assemblies located within the nanometer-scaled interlayer spacing.

2.3 The sheet-scrolling mechanism

Inspired by the above experimental results, we propose a binding formation scheme and a sheet-scrolling mechanism, as presented in Fig. 5. After intercalating into the interlayer spacing of $Ti_3C_2T_x$, AA molecules undergo oxidization (possibly involved in the electrochemical process from C–Ti–O to C–Ti–OH,[50] Table S3†) and adsorption onto the $Ti_3C_2T_x$ surface *via* the C–O–Ti bidentate or monodentate coordination bond. Besides the bonding with $Ti_3C_2T_x$, AA molecules themselves interact and link with each other *via* hydrogen bonding to form large assemblies within the interlayer spacing. Lattice deformation caused by each bidentate or monodentate bonding formation might be slight or even negligible on the original crystalline structure of pristine $Ti_3C_2T_x$. However, when enough AA

molecules are intercalated to form large and quantitatively enough assemblies, the slight lattice deformation caused by each bonding could line up orderly along the hydrogen bonding pathway where internal stress adds up until a certain bending threshold is reached. The effect of the lattice deformation is to facilitate the bending/scrolling up of the MXene sheets. Together with the diminished electrostatic repulsion after AA addition, the $Ti_3C_2T_x$ nanosheets, composed of three layers of titanium atoms and two layers of carbon atoms, finally are corrugated, curled, and eventually scrolled up into fibers to reduce surface energy. The bending/scrolling-up direction of each MXene nanosheet should be random (as shown in Fig. 5, it could be upward or downward); after twisted MXene strips or fibers are formed, the rest MXene sheets would wrap around those strips and fibers. One thing to note is that sonication is indispensable to obtaining fibers (Fig. S8†). Sonication here might promote intercalation and formation of C–O–Ti (see Fig. S9 and Table S3†) as well as introducing defects to facilitate the scrolling process. Moreover, the fiber formation process is irreversible. After removing AA from $M_{10}AA_{10}$ and then repeatedly adding AA, the fibers cannot be obtained again, probably due to the stacking of MXene sheets resulting from the previous fiber formation process (Fig. S10†).

2.4 Electrical and mechanical properties

We studied the effects of AA on the electrical conductivity and mechanical properties of the as-prepared MXene-fiber sponges. The electrical conductivity is measured by four-point probe resistivity measurements after pressing the $M_{10}AA_x$ sponges under 100 kPa. The electrical conductivity of the as-prepared $M_{10}AA_x$ decreased from 3112 S cm^{-1} of $M_{10}AA_0$ (close to other reported values[25]) to 0.01 S cm^{-1} of $M_{10}AA_{25}$ (Fig. 6a), which is quite
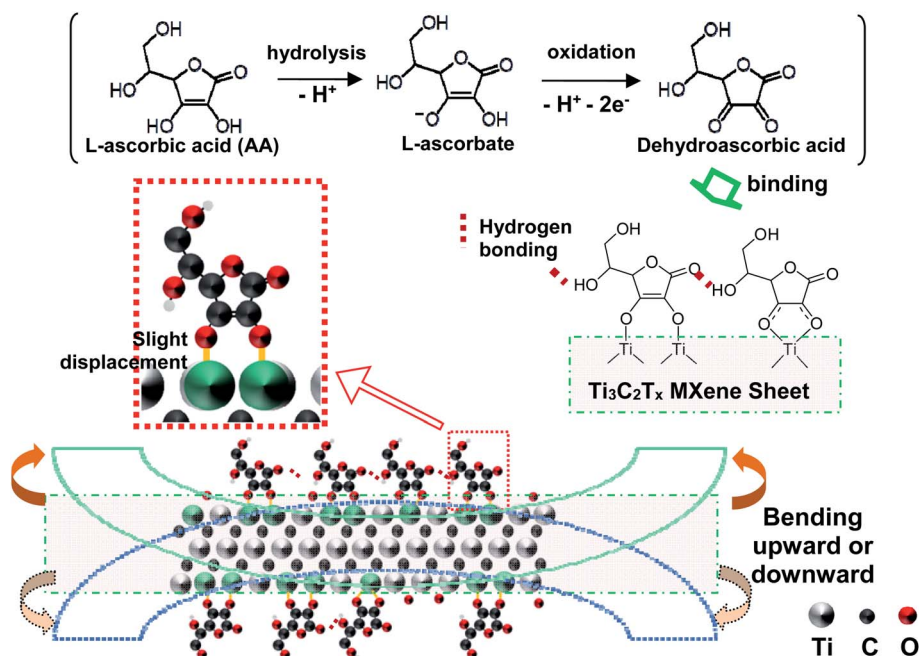

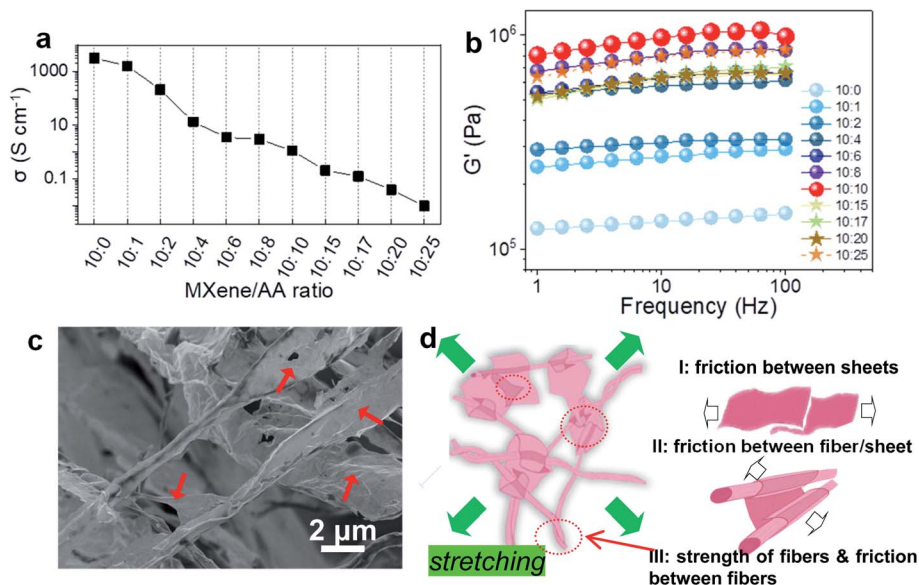**Fig. 5** The proposed binding formation and sheet-scrolling mechanism.

Fig. 6 (a) The electrical conductivity of $M_{10}AA_x$ with different AA ratios; (b) storage modulus G' vs. frequency of $M_{10}AA_x$ with different AA ratios at the constant stain of 0.1%; (c) $M_{10}AA_{10}$ shows unrolled $Ti_3C_2T_x$ sheets (red arrowed) wrapped around fibers; (d) schematic illustration of strengthening mechanism in $M_{10}AA_{10}$.

reasonable as a result of the non-conductive AA molecules intercalated and/or deposited on the surface of the $Ti_3C_2T_x$. Notwithstanding, it might be inspirational for application in electronics or energy storage devices to find other types of chemicals that can not only scroll up the MXene nanosheets in a similar way but also are electro-conductive or pseudo-capacitive.

The $M_{10}AA_x$ sponges exhibit a darkening color as well as a relatively more rigid texture as increasing the AA ratio (Fig. S2†); meanwhile, the specific surface area decreases as MXene nanosheets are scrolled up into fibers, and then fibers twine around each other to form even thicker fibers (Fig. S12 and Table S5†). Due to the sponges' soft texture, we use the rheological testing technique instead of standard tensile testing methods. The as-synthesized 2 cm-thick sponge was pressed to 1000 μm thick for the measurements. The storage modulus (G'), also known as Young's modulus, *versus* the frequency of different $M_{10}AA_x$ sponges, is plotted in Fig. 6b. The storage modulus experiences a course of "increase (I)–drop–increase (II)": the pure MXene sponge ($M_{10}AA_0$) admits a storage modulus of ~123 kPa at 1 Hz (maximum ~145 kPa) and increases to ~805 kPa (maximum ~1053 kPa) by nearly 7 folds when the MXene/AA ratio is 10 : 10, then drops to ~510 kPa (maximum ~655 kPa) at 10 : 15 and turns back to increase until 632 kPa (maximum ~844 kPa) at 10 : 25. Increase (I) should be the result of MXene sheets being scrolled up into strips with higher mechanical rigidity and toughness. Increase (II) is ascribed to the thickening of the fiber bundles. The most interesting fact is the maximum G' admitted by $M_{10}AA_{10}$, which we conjecture, is the result of the unique morphology co-comprised of both fibers and non-scrolled $Ti_3C_2T_x$ sheets attached to those fibers (Fig. 2a and 6c). The fibers act as skeletons while the $Ti_3C_2T_x$ sheets act as inter-fiber linkages and provide extra frictional sliding between contacting sheets

(Fig. 6d), similar to two-dimensional graphene working as composite reinforcement, which can significantly enhance the strength and toughness of the polymeric matrices.[51]

3. Conclusions

In this study, we have realized scrolling up $Ti_3C_2T_x$ sheets into tightly-scrolled fibers using AA as an intercalant and bending agent. The proposed sheet-scrolling mechanism well explains the phenomenon that lattice deformation induced by AA assemblies builds up as increasing the AA ratio, combined with the reduced electrostatic repulsion, eventually leads to spontaneous scrolling of $Ti_3C_2T_x$ sheets. Through changing the MXene/AA ratio, the diameter of the as-obtained fibers can be tuned from ~500 nm to ~3 μm. It also enables us to tailor the mechanical properties of the materials by changing their microstructures, such as the existence of fibers, the diameter of the fibers, and the proportion of fibers to non-scrolled $Ti_3C_2T_x$ sheets. The electrical conductivity of our AA-treated MXene fibers can also be tuned depending on different applications. Nonetheless, this finding opens an avenue for exploring a variety of other compounds for curling, scrolling up $Ti_3C_2T_x$ and other types of MXenes into fibers, and therefore offers new possibilities and approaches to fiber-shaping MXene for versatile applications including structural composites, flexible electronics, and many others.

4. Experimental

4.1 Synthesis of delaminated $Ti_3C_2T_x$ MXene

$Ti_3C_2T_x$ was prepared using the mild etching method. In a typical procedure, 0.5 g of LiF (Alfa Aesar, 99.98%) was slowly added into 5 ml of 9 M HCl (Sinopharm, AR grade) solution while stirring, then 0.5 g of Ti_3AlC_2 (Innochem, 200 mesh) was

slowly added in for 15 min. The above mixture was then kept at 35 °C for 48 h under continuous stirring. Afterwards, the reacted mixture was washed using deionized (DI) water and centrifuged at 3500 rpm until the pH reached approximately 6. The obtained dispersion then underwent probe sonication (135 W) in the iced bath for 30 min under Ar bubbling. Finally, the delaminated $Ti_3C_2T_x$ was collected by centrifugation at 10 000 rpm for 1 h.

4.2 Preparation of AA-treated MXene

The as-synthesized $Ti_3C_2T_x$ MXene was re-dispersed to 2 mg ml^{-1}. Then ascorbic acid (AA, Innochem, 99%) was added to the weight ratio of MXene : AA = 10 : 0, 10 : 1, 10 : 2, 10 : 4, 10 : 6, 10 : 8, 10 : 10, 10 : 15, 10 : 17, 10 : 20, and 10 : 25 followed by stirring for 30 min and probe sonication in the iced bath for 15 min at 135 W under Ar bubbling and denoted as $M_{10}AA_x$ solution. After ~24 h freeze-drying, the AA-treated MXene sponges were obtained and named as $M_{10}AA_x$, where x represented the mass ratio of AA.

4.3 NaHCO₃ adjustment of $M_{10}AA_{10}$

60 mg ml^{-1} of NaHCO₃ (Aladdin, 99.8%) solution was added to the $M_{10}AA_{10}$ solution under stirring and Ar bubbling until the pH increased and stabilized at 4, 5, 6, 7, and 8, respectively. The pH of the solution was measured at room temperature. Then after probe sonication (135 W) in the iced bath for 15 min under Ar bubbling, the NaHCO₃ treated $M_{10}AA_{10}$ were obtained after freeze-drying.

4.4 Acid treatment of MXene

HCl (Sinopharm, AR grade) and HAc (Sigma-Aldrich, 99.7%) were added to the $Ti_3C_2T_x$ MXene solution (2 mg ml^{-1}) until the pH of the finishing mixed solution was the same as $M_{10}AA_{10}$. Then after the same stirring and probe sonication procedure, the HCl and HAc treated MXene sponges were obtained after freeze-drying.

4.5 Removing and repeatedly adding AA

The as-prepared $M_{10}AA_{10}$ sponge was dissolved in DI water, then washed with DI water using a centrifuge at 3500 rpm until the pH was ~6 (named AA-rm), and added AA again with the MXene/AA ratio of 10 : 10 (named AA-rpt). After the same stirring and probe sonication procedure, the AA-rm and AA-rpt treated MXene sponges were obtained after freeze-drying.

4.6 Material characterization

The SEM images were obtained on a Zeiss crossbeam 550, Germany, and the TEM images on a JEM-F200, Japan. Raman was performed with an excitation light source of 532 nm. The laser power used in the measurements was 50 mW, and the exposure time was 30 s. XRD data were collected using an X-ray powder diffractometer (D/MAX-γA, Japan, $\lambda = 1.54$ Å) with a step size of 0.02°. FTIR was carried out using a Fourier transform infrared spectrometer (Vertex 80 + Hyperion 2000, Germany) to investigate the chemical structure of the samples. The single-layer thickness of the delaminated $Ti_3C_2T_x$ was obtained by

AFM (atomic force microscope, Hitachi 5500M, Japan). XPS spectra (X-ray photoelectron spectroscopy) were obtained on an ESCALAB 250Xi, America; zeta potential analyzer (Zetasizer nano, England) was used to measure the zeta potential, and the sample concentration was 0.1 mg ml^{-1}. The electrical conductivity test was carried out using a digital four-probe tester (ST-2258C, China), and the samples were prepared by pressing $M_{10}AA_x$ sponges of ~4 mm to ~6 mm thickness (thickness variation due to different AA ratios) under 100 kPa. The rheological property of $M_{10}AA_x$ was measured on a TA hybrid rheometer (HR-1, America) after pressing the $M_{10}AA_x$ sponge from a thickness of ~2 cm to 1 mm. Nitrogen sorption measurements were conducted on a Quadrasorb instrument (Quantachrome, Autosorb IQ-MP-MP, USA) at 77 K using liquid nitrogen to determine the specific surface area and pore size distribution. All samples were tested after degassing at 70 °C in a vacuum for 12 h. The pore size distributions were calculated by the density functional theory (DFT) method.

Author contributions

J. C. fabricated, characterized, and analyzed the data. Y. W. and Q. Z. imaged the scrolling process and the frictional sliding process. J. Y. and J. C. performed the zeta potential tests. B. W. discussed the results. Q. Z. developed the idea and supervised the projects. J. C., B. W., and Q. Z. wrote the manuscript. All authors discussed the results and comments on the final version of the manuscript.

Conflicts of interest

The authors declare no competing financial interest.

Acknowledgements

Notes and references

1 A. Lipatov, H. D. Lu, M. Alhabeb, B. Anasori, A. Gruverman, Y. Gogotsi and A. Sinitskii, *Sci. Adv.*, 2018, **4**, 0491.
2 K. S. Novoselov, V. I. Fal'ko, L. Colombo, P. R. Gellert, M. G. Schwab and K. Kim, *Nature*, 2012, **490**, 192–200.
3 B. Anasori, Y. Xie, M. Beidaghi, J. Lu, B. C. Hosler, L. Hultman, P. R. C. Kent, Y. Gogotsi and M. W. Barsoum, *ACS Nano*, 2015, **9**, 9507–9516.
4 B. Anasori, M. R. Lukatskaya and Y. Gogotsi, *Nat. Rev. Mater.*, 2017, **2**, 1–17.
5 V. Strauss, K. Marsh, M. D. Kowal, M. El-Kady and R. B. Kaner, *Adv. Mater.*, 2018, **30**, 1704449.
6 X. Li, J. G. Yu, S. Wageh, A. A. Al-Ghamdi and J. Xie, *Small*, 2016, **12**, 6640–6696.

7   T. L. Li, X. Y. Jiao, T. You, F. Dai, P. P. Zhang, F. Yu, L. Hu, L. W. Ding, L. Zhang, Z. B. Wen and Y. P. Wu, *Ceram. Int.*, 2019, **45**, 4283–4289.

8   Y. H. Wang, K. J. Huang and X. Wu, *Biosens. Bioelectron.*, 2017, **97**, 305–316.

9   M. Naguib, M. Kurtoglu, V. Presser, J. Lu, J. J. Niu, M. Heon, L. Hultman, Y. Gogotsi and M. W. Barsoum, *Adv. Mater.*, 2011, **23**, 4248–4253.

10 X. Q. Xie, M. Q. Zhao, B. Anasori, K. Maleski, C. E. Ren, J. W. Li, B. W. Byles, E. Pomerantseva, G. X. Wang and Y. Gogotsi, *Nano Energy*, 2016, **26**, 513–523.

11 C. F. Zhang, B. Anasori, A. Seral-Ascaso, S. Park, N. McEvoy, A. Shmeliov, G. S. Duesberg, J. N. Coleman, Y. Gogotsi and V. Nicolosi, *Adv. Mater.*, 2017, **29**, 1702678.

12 M. Q. Zhao, X. Q. Xie, C. E. Ren, T. Makaryan, B. Anasori, G. X. Wang and Y. Gogotsi, *Adv. Mater.*, 2017, **29**, 1702410.

13 X. H. Wu, Z. Y. Wang, M. Z. Yu, L. Y. Xiu and J. S. Qiu, *Adv. Mater.*, 2017, **29**, 1607017.

14 L. Liu, G. B. Ying, C. Hu, K. C. Zhang, F. C. Ma, L. Su, C. Zhang and C. Wang, *ACS Appl. Nano Mater.*, 2019, **2**, 5553–5562.

15 H. Wang and J. M. Lee, *J. Mater. Chem. A*, 2020, **8**, 10604–10624.

16 N. Murugan, R. Jerome, M. Preethika, A. Sundaramurthy and A. K. Sundramoorthy, *J. Mater. Sci. Technol.*, 2021, **72**, 122–131.

17 Q. Wang, X. Xiao, X. Hu, L. Huang, T. Li and M. Yang, *Mater. Lett.*, 2021, **285**, 129158.

18 X. Jiang, A. V. Kuklin, A. Baev, Y. Ge, H. Agren, H. Zhang and P. N. Prasad, *Phys. Rep.*, 2020, **848**, 1–58.

19 T. Yun, H. Kim, A. Iqbal, Y. S. Cho, G. S. Lee, M. K. Kim, S. J. Kim, D. Kim, Y. Gogotsi, S. O. Kim and C. M. Koo, *Adv. Mater.*, 2020, **32**, 1906769.

20 J. Z. Zhang, N. Kong, S. Uzun, A. Levitt, S. Seyedin, P. A. Lynch, S. Qin, M. K. Han, W. R. Yang, J. Q. Liu, X. G. Wang, Y. Gogotsi and J. M. Razal, *Adv. Mater.*, 2020, **32**, 2001093.

21 Y. Z. Chen, Y. Q. Ge, W. C. Huang, Z. J. Li, L. M. Wu, H. Zhang and X. J. Li, *ACS Appl. Nano Mater.*, 2020, **3**, 303–311.

22 A. S. Levitt, M. Alhabeb, C. B. Hatter, A. Sarycheva, G. Dion and Y. Gogotsi, *J. Mater. Chem. A*, 2019, **7**, 269–277.

23 Z. H. Zhou, W. Panatdasirisuk, T. S. Mathis, B. Anasori, C. H. Lu, X. X. Zhang, Z. W. Liao, Y. Gogotsi and S. Yang, *Nanoscale*, 2018, **10**, 6005–6013.

24 J. Z. Zhang, S. Seyedin, S. Qin, Z. Y. Wang, S. Moradi, F. L. Yang, P. A. Lynch, W. R. Yang, J. Q. Liu, X. G. Wang and J. M. Razal, *Small*, 2019, **15**, 1804732.

25 N. F. He, S. Patil, J. G. Qu, J. Y. Liao, F. Zhao and W. Gao, *ACS Appl. Energy Mater.*, 2020, **3**, 2949–2958.

26 Q. Guo, T. Wu, L. Liu, H. Hou, S. Chen and L. Wang, *J. Mater. Chem. B*, 2018, **6**, 4610–4617.

27 J. Z. Zhang, S. Uzun, S. Seyedin, P. A. Lynch, B. Akuzum, Z. Y. Wang, S. Qin, M. Alhabeb, C. E. Shuck, W. W. Lei, E. C. Kumbur, W. R. Yang, X. G. Wang, G. Dion, J. M. Razal and Y. Gogotsi, *ACS Cent. Sci.*, 2020, **6**, 254–265.

28 S. Li, Z. D. Fan, G. Q. Wu, Y. Y. Shao, Z. Xia, C. H. Wei, F. Shen, X. L. Tong, J. C. Yu, K. Chen, M. L. Wang, Y. Zhao, Z. P. Luo, M. Q. Jian, J. Y. Sun, R. B. Kaner and Y. L. Shao, *ACS Nano*, 2021, **15**, 7821–7832.

29 L. M. Viculis, J. J. Mack and R. B. Kaner, *Science*, 2003, **299**, 1361–1362.

30 M. V. Savoskin, V. N. Mochalin, A. P. Yaroshenko, N. I. Lazareva, T. E. Konstantinova, I. V. Barsukov and I. G. Prokofiev, *Carbon*, 2007, **45**, 2797–2800.

31 M. Alhabeb, K. Maleski, B. Anasori, P. Lelyukh, L. Clark, S. Sin and Y. Gogotsi, *Chem. Mater.*, 2017, **29**, 7633–7644.

32 M. Malaki, A. Malekib and R. S. Varma, *J. Mater. Chem. A*, 2019, **7**, 10843–10857.

33 Y. Z. Fang, R. Hu, K. Zhu, K. Ye, J. Yan, G. L. Wang and D. X. Cao, *Adv. Funct. Mater.*, 2020, **30**, 2005663.

34 A. Vaughn, J. Ball, T. Heil, D. J. Morgan, G. I. Lampronti, G. Maršalkaitė, C. L. Raston, N. P. Power and S. Kellici, *Chem.–Eur. J.*, 2017, **23**, 8128–8133.

35 J. N. Meng, F. F. Zhang, L. Zhang, L. Y. Liu, J. T. Chen, B. J. Yang and X. B. Yan, *J. Energy Chem.*, 2020, **46**, 256–263.

36 C. W. Wu, B. Unnikrishnan, I. W. P. Chen, S. G. Harroun, H. T. Chang and C. C. Huang, *Energy Storage Mater.*, 2020, **25**, 563–571.

37 X. F. Zhao, A. Vashisth, E. Prehn, W. M. Sun, S. A. Shah, T. Habib, Y. X. Chen, Z. Y. Tan, J. L. Lutkenhaus, M. Radovic and M. J. Green, *Matter*, 2019, **1**, 513–526.

38 X. Yang, Y. W. Yao, Q. Wang, K. Zhu, K. Ye, G. L. Wang, D. X. Cao and J. Yan, *Adv. Funct. Mater.*, 2021, 2109479.

39 J. Yan, C. E. Ren, K. Maleski, C. B. Hatter, B. Anasori, P. Urbankowski, A. Sarycheva and Y. Gogotsi, *Adv. Funct. Mater.*, 2017, **27**, 1701264.

40 O. Mashtalir, M. Naguib, V. N. Mochalin, Y. Dall'Agnese, M. Heon, M. W. Barsoum and Y. Gogotsi, *Nat. Commun.*, 2013, **4**, 1–7.

41 G. S. Lee, T. Yun, H. Kim, I. H. Kim, J. Choi, S. H. Lee, H. J. Lee, H. S. Hwang, J. G. Kim, D. Kim, H. M. Lee, C. M. Koo and S. O. Kim, *ACS Nano*, 2020, **14**, 11722–11732.

42 J. Halim, K. M. Cook, M. Naguib, P. Eklund, Y. Gogotsi, J. Rosen and M. W. Barsoum, *Appl. Surf. Sci.*, 2016, **362**, 406–417.

43 M. Rodenstein, S. Zürcher, S. G. P. Tosatti and N. D. Spencer, *Langmuir*, 2010, **26**, 16211–16220.

44 J. Saiz-Poseu, J. Mancebo-Aracil, F. Nador, F. Busqué and D. Ruiz-Molina, *Angew. Chem. Int. Edit.*, 2019, **58**, 696–714.

45 K. Syres, A. Thomas, F. Bondino, M. Malvestuto and M. Grätzel, *Langmuir*, 2010, **26**, 14548–14555.

46 A. Sarycheva and Y. Gogotsi, *Chem. Mater.*, 2020, **32**, 3480–3488.

47 Y. Ou, J. D. Lin, H. M. Zou and D. W. Liao, *J. Mol. Catal. A: Chem.*, 2005, **241**, 59–64.

48 M. M. Sk, C. Y. Yue and R. K. Jena, *Polymer*, 2014, **55**, 798–805.

49 M. M. Sk and C. Y. Yue, *J. Mater. Chem. A*, 2014, **2**, 2830–2838.

50 M. R. Lukatskaya, S. Bak, X. Yu, X. Yang, M. W. Barsoum and Y. Gogotsi, *Adv. Energy Mater.*, 2015, **5**, 1500589.

51 H. Kim, A. A. Abdala and C. W. Macosko, *Macromolecules*, 2010, **43**, 6515–6530.